

1     **Does global warming cause intensified interannual**  
2                     **hydroclimate variability?**

3                     RICHARD SEAGER \*   AND NAOMI NAIK

*Lamont Doherty Earth Observatory of Columbia University, Palisades, New York<sup>†</sup>*

4                     LAURA VOGEL

*Columbia College, New York, New York*

---

\* *Corresponding author address:* Richard Seager, Lamont Doherty Earth Observatory of Columbia University, 61 Route 9W., Palisades, NY 10964.

E-mail: seager@ldeo.columbia.edu

<sup>†</sup>LDEO Contribution number xxxx

## ABSTRACT

6 The idea that global warming leads to more droughts and floods has become commonplace  
7 without clear indication of what is meant by this statement. Here we examine one aspect  
8 of this problem and assess whether interannual variability of precipitation ( $P$ ) minus evapo-  
9 ration ( $E$ ) becomes stronger in the 21<sup>st</sup> Century compared to the 20<sup>th</sup> Century, as deduced  
10 from an ensemble of models participating in Coupled Model Intercomparison Project 3. It is  
11 shown that indeed interannual variability of  $P - E$  does increase almost everywhere across  
12 the planet with a few notable exceptions such as southwestern North America and some  
13 subtropical regions. The variability increases most at the Equator and the high latitudes  
14 and least in the subtropics. While most interannual  $P - E$  variability arises from internal  
15 atmosphere variability the primary potentially predictable component is related to the El  
16 Niño-Southern Oscillation (ENSO). ENSO-driven interannual  $P - E$  variability clearly in-  
17 creases in amplitude in the tropical Pacific but elsewhere the changes are more complex.  
18 This is not surprising in that ENSO-driven  $P - E$  anomalies are primarily caused by cir-  
19 culation anomalies combining with the climatological humidity field. As climate warms and  
20 the specific humidity increases this term leads to an intensification of ENSO-driven  $P - E$   
21 variability. However, ENSO-driven circulation anomalies also change, in some regions ampli-  
22 fying, but in others opposing and even overwhelming, the impact of rising specific humidity.  
23 Consequently there is sound scientific basis for anticipating a general increase in interannual  
24  $P - E$  variability but the predictable component will depend in a more complex way on  
25 both thermodynamic responses to global warming and on how tropically-forced circulation  
26 anomalies alter.

## 1. Introduction

According to projections with climate models global warming driven by rising greenhouse gas concentrations will cause significant changes in the distribution of precipitation ( $P$ ) minus evaporation ( $E$ ) at the Earth's surface. These can be summarized as dry areas getting drier and wet areas getting wetter and a poleward and equatorward expansion of the subtropical dry zones. These changes arise from intensified atmospheric moisture transports in a warmer, more moist, atmosphere and a poleward expansion of Hadley Cell, poleward shift of the mid-latitude storm tracks and equatorward contraction of convergence zones (Held and Soden 2006; Seager et al. 2007; Intergovernmental Panel on Climate Change 2007; Neelin et al. 2006; Chou et al. 2009; Seager et al. 2010c). These changes in  $P - E$  will create problems in water-stressed arid zones as well as add to flooding hazards in regions expected to get wetter. However, natural climate variability on day-to-day, month-to-month, year-to-year and decade-to-decade timescales already causes havoc in terms of agricultural losses, transportation disruption by storms, shortfalls in municipal water supply, flooding in low-lying areas, death by starvation following disrupted food availability or in heat waves and so on. Recent examples of disruption, suffering and death caused by climate events that, if not entirely unsullied by the influence of anthropogenic climate change contain a large component of natural climate variability, are the intensely cold and snowy 2009/10 winter in the eastern U.S. and northwest Europe (Seager et al. 2010b; Cattiaux et al. 2010), the Pakistan floods (Webster et al. 2011) and Russian heat wave (Dole et al. 2011) of summer 2010, the intense flooding in northeast Australia early in 2011 and the China drought of winter 2010/11. While it is clearly important to develop means to adapt to long term climate trends a strong case can be made that developing resilience to the worst challenges that natural climate variability can pose will, in and of itself, create a basic level of resilience to anthropogenic climate change (Sarachik 2011). Indeed, for countries such as Pakistan, where whole communities were washed away in the 2010 monsoon floods, it makes little sense to adapt to a multidecadal timescale trend when the countries' infrastructure is so severely stressed by already-existing (dominantly natural) year-to-year variability.

As Sarachik (2011) says 'mitigation is about climate trends, adaptation is about climate

56 variability'. But this does not let climate change off the hook in terms of adaptation. There  
57 is a growing sense that a purely 'natural', i.e. uninfluenced by human activity, climate system  
58 no longer exists and it is widely assumed that climate events like heat waves, stormy winters,  
59 droughts and floods, bear at least some imprint of human-induced climate change rendering  
60 the term 'natural climate variability' a relic of the pre-industrial age. It is commonly stated,  
61 for example, that global warming will simultaneously lead to more floods and droughts and  
62 more climate extremes. As a fairly typical example of common assumptions, writing in  
63 the *New York Times* on August 15 2010, Justin Giles stated 'Theory suggests that a world  
64 warming up ..... will feature heavier rainstorms in summer, bigger snowstorms in winter,  
65 more intense droughts in at least some places and more record-breaking heat waves'. That  
66 is, global warming will lead to more extreme climate variability on all timescales.

67 Increases in atmospheric humidity associated with warming provide a rationale for these  
68 assumptions: any given circulation anomaly can draw on more moisture than before and  
69 create more precipitation. This argument is used to explain observed increases in the pro-  
70 portion of total precipitation falling in the most intense events (Trenberth et al. 2003;  
71 Groisman et al. 2005) although to our knowledge proof of this assertion has not yet been  
72 forthcoming. However, if this is so on short timescales of days or less, the same process  
73 should work on interannual timescales. For example ENSO-related  $P - E$  anomalies and  
74 tropical Pacific forced decadal precipitation changes are fundamentally driven by changes in  
75 circulation acting on the climatological humidity field (Huang et al. (2005); Seager (2007);  
76 Seager and Naik (2011) and below). As specific humidity rises these same forced circulation  
77 anomalies should cause more intensified  $P - E$  variability and, hence, more extreme droughts  
78 and floods.

79 But does interannual  $P - E$  variability intensify as climate warms? Given that interan-  
80 nual  $P - E$  variability is forced by circulation anomalies it is possible that changes in SST  
81 variability or atmosphere dynamics could also create changes in  $P - E$  variability that offset,  
82 or maybe amplify, the expected increase due to thermodynamic processes alone. While adap-  
83 tation to climate variability is a good first step towards adaptation to climate change it needs  
84 to be known what climate variability to adapt to. Most countries in the world are already  
85 stressed by climate variability (including wealthy ones with well developed infrastructure as

86 evidenced by, for example, drought in the southeast U.S. in 2006/7 (Seager 2007) and floods  
87 in the U.K. in 2000 (Pall et al. 2011)) and if global warming causes the variability to get  
88 more extreme this needs to be known. That is what we examine here focusing on the year-  
89 to-year timescale. On this timescale the dominant mode of global  $P - E$  variability is the  
90 El Niño-Southern Oscillation (ENSO). We will examine the Coupled Model Intercomparison  
91 Project 3 (CMIP3) archive used by the Intergovernmental Panel on Climate Change (IPCC)  
92 Assessment Report 4 (AR4) (Meehl et al. 2007) using simulations of the 20th Century and  
93 projections of the current century in all the models that make all the needed data avail-  
94 able. We will look at how ENSO-related  $P - E$  variability changes and separate this into  
95 changes in the dynamic (caused by circulation anomalies) and thermodynamic (caused by  
96 humidity anomalies) components and then look at how these contributions change between  
97 the centuries and, to the extent we can, why.

98 Increased amplitude of interannual variability as a consequence of global warming would  
99 create new problems for societies struggling to adapt to already-existing interannual vari-  
100 ability. This would be in addition to any additional challenges posed by trends in the mean  
101 climate state and, on the floods side, changes in land use and population within the catch-  
102 ment and flood plains. As we will show, model projections of current century climate show  
103 a widespread but not universal increase in the amplitude of the total interannual variability  
104 of  $P - E$  and of the ENSO-driven component in many places. However, in some regions  
105 changes in circulation variability offset changes due to increasing humidity leading to little  
106 change in, or even reduced, amplitude of  $P - E$  variability.

## 107 **2. Model data used and methodology**

108 We analyze 19 models from the CMIP3/IPCC AR4 archive. The models were selected  
109 because all of the needed data were available and free of errors. We analyze both the 20<sup>th</sup>  
110 Century simulations with known and estimated past climate forcings and the projections of  
111 21<sup>st</sup> Century climate using the 'middle-of-the-road' SResA1B emissions scenario. In prior  
112 work (Seager et al. (2010a); Seager and Naik (2011) ; hereafter SN) we have analyzed only  
113 those models and time periods for which all the daily data needed to evaluate transient eddy

114 moisture convergences were available (1961-2000 and 2046-65). SN showed that ENSO-  
115 forced  $P - E$  variability is dominated in these CMIP3/IPCC AR4 models by changes in  
116 the mean circulation combining with the climatological moisture field to create anomalous  
117 convergence and divergence of moisture. They found that contributions from both variability  
118 in humidity and changes in moisture convergence or divergence by transient eddies (defined  
119 as co-variances of submonthly wind and specific humidity fields) were decidedly of secondary  
120 importance. Here we do not seek to evaluate changes in the variability of transient eddy  
121 moisture convergence and divergence which means we do not need daily data. This allows us  
122 to improve the characterization of contributions to  $P - E$  variability from changes in mean  
123 quantities by using the entire two centuries of modeled data and allows an expansion from  
124 15 to 19 models. 5 of the 24 CMIP3/IPCC AR4 models available were not used, 3 because of  
125 lack of needed data and 2 because their natural variability was blatantly unrealistic. Included  
126 and excluded models are listed in Table 1.

127 We begin with the vertically integrated moisture budget equation which balances  $P - E$   
128 with convergence of moisture by the mean and transient flow, viz:

$$\rho_w g (\overline{P} - \overline{E}) \approx - \int_0^{\overline{p}_s} (\nabla \cdot (\overline{\mathbf{u}}\overline{q} + \overline{\mathbf{u}}\hat{q} + \hat{\mathbf{u}}\overline{q})) dp - \int_0^{\overline{p}_s} \nabla \cdot (\overline{\mathbf{u}'q'}) dp - \overline{q_s \mathbf{u}_s \cdot \nabla p_s}, \quad (1)$$

129 Here  $E$  is understood to be evaporation over the ocean and evapotranspiration over land. In  
130 Equation 1 the climatological monthly mean quantities are represented by double overbars,  
131 monthly means by single overbars, monthly departures from the climatological monthly  
132 mean by hats and departures from monthly means by primes. Total fields are given by, for  
133 example,  $\mathbf{u} = \overline{\mathbf{u}} + \mathbf{u}' = \overline{\mathbf{u}} + \hat{\mathbf{u}} + \mathbf{u}'$ . Products of monthly anomalies have been neglected.  
134  $\rho_w$  is water density,  $g$  is the acceleration due to gravity,  $p$  is pressure,  $p_s$  surface pressure,  $\mathbf{u}$   
135 is the horizontal vector wind and  $\mathbf{u}_s$  its surface value and  $q$  is specific humidity. The first  
136 term on the right hand side is the horizontal moisture convergence by the mean flow and the  
137 second term the horizontal moisture convergence by the submonthly transient eddies. (The  
138 third term provides a general tendency to reduce  $P - E$  (because of surface flow down the  
139 pressure gradient) but cannot be evaluated for all models since many did not save daily values  
140 of surface winds and humidity. Within the GFDL CM2.1 model this term was evaluated

141 with daily data and then found to be reasonably approximated using monthly data. We then  
 142 evaluated it for all models using monthly data. It is several times smaller than the other  
 143 two terms and we discuss it no more.)

144 The dominant mode by far of global  $P - E$  variability is ENSO. Hence we will focus on  
 145 potential changes in the interannual variability of ENSO-forced  $P - E$  variability. We break  
 146 down the moisture budget into a term related to variability in circulation and a term related  
 147 to variability in humidity, variability in transient eddy moisture convergence and variability  
 148 in the boundary term. Introducing the notation:

$$\langle \mathbf{A} \rangle^T = \int_0^{\bar{p}_s, T} (\nabla \cdot \mathbf{A}) dp. \quad (2)$$

The superscript  $T$  indicates the time period, i.e. 20<sup>th</sup> or 21<sup>st</sup> Century, corresponding to the pressure data for the vertical integral. Below the subscript  $T$  indicates a time period for the subscripted variable. Then we have for the case of ENSO variability:

$$\rho_w g \delta(\bar{P} - \bar{E}) \approx \delta TH + \delta MCD + \delta TE - \delta S, \quad (3)$$

$$\delta TH = -\delta \langle \bar{\mathbf{u}}_T \hat{q}_T \rangle^T, \quad (4)$$

$$\delta MCD = -\delta \langle \hat{\mathbf{u}}_T \bar{q}_T \rangle^T, \quad (5)$$

$$\delta TE = -\delta \langle (\bar{\mathbf{u}}' q')_T \rangle^T, \quad (6)$$

$$\delta S = \delta \langle \overline{(q_s \mathbf{u}_s \cdot \nabla p_s)}_T \rangle. \quad (7)$$

The term influenced only by changes in humidity is called the thermodynamic term,  $\delta TH$  and the term influenced only by changes in the mean circulation is called the dynamic term,  $\delta MCD$ .  $\delta TE$  is the term related to changes in transient eddy fluxes and  $\delta S$  is the change in the boundary term. The difference  $\delta$ , is given by:

$$\delta(\cdot) = [\cdot]_{LN} - [\cdot]_{EN}, \quad (8)$$

149 where the square brackets with subscripts LN and EN indicate time-averaging over months  
 150 with La Niña or El Niño conditions of the quantity in parentheses. The approximate equality  
 151 in Eq. 3 assumes that the vertically integrated climatological term is the same averaged over  
 152 El Niño events as over La Niña events despite the differing limits on the pressure integral  
 153 i.e.  $[\langle \bar{\mathbf{u}}_T \bar{q}_T \rangle^T]_{EN} \approx [\langle \bar{\mathbf{u}}_T \bar{q}_T \rangle^T]_{LN}$ .

154 El Niño and La Niña conditions are found by conducting an Empirical Orthogonal Func-  
155 tion (EOF) analysis of the annual mean  $P - E$  field in each model and for each century, after  
156 detrending to remove the century-long trends. Since ENSO events tend to be centered on  
157 the boreal winter season the annual mean is defined on a July to June year. Defining ENSO  
158 using  $P - E$  is unorthodox but makes sense in that  $P - E$ , rather than ocean temperature,  
159 is our interest here.  $P - E$  variance is also concentrated in the tropics and hence ENSO  
160 variability is easily located in this manner. Indeed, in all models the first EOF is the model's  
161 representation of ENSO, centered in the tropical Pacific and explaining between 15 to 49%  
162 of the total variance of  $P - E$  with a mean of 32%, comparable to that observed (see SN). To  
163 compute La Niña minus El Niño differences we take the associated principal component for  
164 each model and compute composites over all years when it exceeds one standard deviation  
165 and all years over which it is below one standard deviation. This difference is the La Niña  
166 minus El Niño composite difference. Here we only show the multimodel ensemble mean  
167 (MEM) of the composite differences.

168 To analyze the change in the  $P - E$  variability we will need to determine what causes  
169 20<sup>th</sup> to 21<sup>st</sup> Century changes in the  $MCD$  and  $TH$  contributions, i.e. how changes in the  
170 mean and variability of specific humidity and circulation cause changes in the dynamic and  
171 thermodynamic drivers of  $P - E$  variability. To do this we define a 21<sup>st</sup> Century minus 20<sup>th</sup>  
172 Century change as:

$$\Delta(\cdot) = (\cdot)_{21} - (\cdot)_{20}, \quad (9)$$

173 where the subscripts 21 and 20 refer to 21<sup>st</sup> and 20<sup>th</sup> Century averages. Hence  $\bar{\mathbf{u}}_{21} = \bar{\mathbf{u}}_{20} + \Delta\bar{\mathbf{u}}$ ,  
174  $\delta\bar{q}_{21} = \delta\bar{q}_{20} + \Delta\delta\bar{q}$ , etc. Hence the change in  $P - E$  variability can be divided up into changes  
175 in the variabilities of the thermodynamic term, the mean circulation dynamics term and the  
176 transient eddy and boundary terms, viz:

$$\rho_w g \Delta(\delta(P - E)) \approx \Delta(\delta TH) + \Delta(\delta MCD) + \Delta(\delta TE) - \Delta(\delta S). \quad (10)$$

177 Substituting the relations for 21<sup>st</sup> and 20<sup>th</sup> Century values into Equation 3, and neglecting  
178 terms nonlinear in  $\Delta$  (such as  $\Delta\bar{\mathbf{u}}\Delta\bar{q}$ ), gives:

$$\Delta(\delta TH) \approx \Delta(\delta TH_q) + \Delta(\delta TH_u), \quad (11)$$

$$\Delta(\delta TH_q) = -\delta\langle\bar{\mathbf{u}}_{20}\Delta\hat{q}\rangle^{21}, \quad (12)$$

$$\Delta(\delta TH_u) = -\delta\langle\Delta\bar{\mathbf{u}}\hat{q}_{20}\rangle^{21}, \quad (13)$$

179 that is, the change in the thermodynamic contribution to  $P - E$  variability involves a term  
 180 (Eq. 12) that is caused by a change in the humidity variability combining with the un-  
 181 changed circulation and a term (Eq. 13) that is caused by a change in the mean circulation  
 182 combining with the unchanged humidity variability. The approximation in Eq. 11 assumes  
 183 that  $\delta\langle\bar{\mathbf{u}}_{20}\hat{q}_{20}\rangle^{21} \approx \delta\langle\bar{\mathbf{u}}_{20}\hat{q}_{20}\rangle^{20}$  which was assessed and found to be valid.

184 Similarly the mean circulation dynamics contribution to the change in  $P - E$  variability  
 185 breaks down as:

$$\Delta(\delta MCD) \approx \Delta(\delta MCD_q) + \Delta(\delta MCD_u), \quad (14)$$

$$\Delta(\delta MCD_q) = -\delta\langle\hat{\mathbf{u}}_{20}\Delta\bar{\bar{q}}\rangle^{21}, \quad (15)$$

$$\Delta(\delta MCD_u) = -\delta\langle\Delta\hat{\mathbf{u}}\bar{\bar{q}}_{20}\rangle^{21}, \quad (16)$$

186 that is, a term (Eq. 15) caused by the change in mean humidity combining with the un-  
 187 changed circulation variability and a term (Eq. 16) caused by a change in the circulation  
 188 variability combining with the unchanged humidity. The approximation in Eq. 14 assumes  
 189 that  $\delta\langle\hat{\mathbf{u}}_{20}\bar{\bar{q}}_{20}\rangle^{21} \approx \delta\langle\hat{\mathbf{u}}_{20}\bar{\bar{q}}_{20}\rangle^{20}$  which was also assessed and found to be valid.

190 At this point it should be noticed that the breakdown of  $P - E$  variability into thermo-  
 191 dynamic and dynamic contributions is no longer absolute. As climate changes and climato-  
 192 logical mean specific humidity and circulation change the efficiency of the thermodynamic  
 193 and dynamic contributions to  $P - E$  variability will change. For example  $P - E$  variability  
 194 that arises from specific humidity variability will differ as the climatological mean circulation  
 195 that converges the humidity anomalies alters. Similarly the increase in climatological mean  
 196 specific humidity accompanying global warming appears in the  $\Delta(MCD_q)$  term where it  
 197 acts to make the circulation variability more effective: i.e. the same amplitude of circulation

198 variability in the 21<sup>st</sup> Century as in the 20<sup>th</sup> Century creates a tendency to larger  $P - E$   
199 variability because it is operating on an enhanced mean moisture field.

### 200 **3. Changes in model simulated total interannual $P - E$** 201 **variability**

202 While the remainder of the paper considers changes in  $P - E$  variability associated with  
203 the leading mode of global  $P - E$  variability, ENSO, we begin with an assessment of how  
204 the total  $P - E$  variability changes. Figure 1 shows the MEM of the variances of annual  
205 mean  $P - E$  of each model for the entire simulated 20<sup>th</sup> Century, the projected 21<sup>st</sup> Century  
206 and the difference. In this case the  $P - E$  variability is contributed to by ENSO, all other  
207 large-scale modes of  $P - E$  variability in the models (e.g. model representations of Atlantic  
208 variability, Indian Ocean sector variability, decadal Pacific variability, the North Atlantic  
209 Oscillation, annular modes etc.) as well as by the smaller scale and higher frequency vari-  
210 ability often referred to as 'noise' in the climate research literature but commonly considered  
211 to be weather. There is a clear increase of interannual  $P - E$  variability over the tropical  
212 Pacific Ocean where ENSO originates. That is, the difference between the positive El Niño  
213 anomalies and negative La Niña anomalies becomes larger in the 21<sup>st</sup> Century as the climate  
214 warms. The percent change in total variance is shown in Figure 2a. An increase in variance  
215 occurs across almost the entire planet with maximum increases in the tropical Pacific and  
216 polar regions. There are regions of decrease over southern North America, Central America,  
217 the subtropical Atlantic Ocean, the equatorial Atlantic Ocean and northeast Brazil and over  
218 parts of the subtropical eastern Pacific Ocean. In addition there is a clear spatial structure  
219 to the change in variance with the largest increases in the equatorial Pacific Ocean and polar  
220 regions and, in general, lesser increases, or decreases, in the subtropics.

221 The most obvious likely cause of a general increase in  $P - E$  variability is the increase  
222 in the climatological mean specific humidity which will allow even unchanged circulation  
223 anomalies to create larger moisture convergence anomalies. The fractional change in the  
224 vertically integrated lower tropospheric specific humidity is shown in Figure 2b. It increases

225 everywhere and has generally the same spatial structure as the increase in  $P - E$  variance  
226 with tropical and high latitude maxima and subtropical minima. The pattern of change in  
227 lower tropospheric water vapor is akin to that of the change in mean  $P - E$  that accompanies  
228 global warming (Held and Soden 2006; Seager et al. 2010c).

229 However, comparing Figures 2a and 2b, it is also clear that the increase in  $P - E$  variance  
230 is in some places markedly less than the change in the mean specific humidity and in others  
231 markedly greater. In work on increases in precipitation intensity it has proven possible to  
232 provide an explanation accounting only for, say, how condensation along a moist adiabat  
233 changes as the atmosphere column warms (O’Gorman and Schneider 2009) while ignoring  
234 changes in vertical velocity. This does not appear to be the case for annual mean  $P - E$   
235 variance. Figures 2c and 2d show that the variances of both the monthly mean and the  
236 annual mean vertical velocities at 700mb decline from the 20<sup>th</sup> to the 21<sup>st</sup> Century almost  
237 everywhere. Areas of increase are limited to the polar regions and the equatorial Pacific  
238 Ocean (and a few other isolated locations).  $P - E$  is inextricably tied to the product  
239 of vertical motion and the specific humidity of the lifted air. For the widespread areas  
240 where the  $P - E$  variance changes less than the increase in mean specific humidity, it is  
241 because the vertical velocity variance decreases. Consequently, for changes in the interannual  
242 variability of  $P - E$ , both changes in the mean specific humidity and changes in the vertical  
243 velocity variance are important. Needless to say the former is easily understood in terms of  
244 moist thermodynamics while there is less understanding of the latter because vertical motion  
245 fields are determined through a complex mix of dynamical and thermodynamical processes  
246 and across a wide range of circulation phenomena. It should also be noted that over land  
247 areas, unlike over the ocean, processes involving soil moisture, groundwater (if included in  
248 the model) and vegetation can influence  $E$  and, hence,  $P$  and water vapor convergence  
249 or divergence, and that these land surface feedbacks can impact circulation and climate  
250 variability (e.g. Koster et al. (2004); Lo and Famiglietti (2011); Seneviratne et al. (2006);  
251 Anyah et al. (2008)).

## 4. Changes in ENSO-driven interannual $P - E$ variability

We now turn our attention to that portion of the total  $P - E$  variability driven by ENSO. Figure 3 shows the La Niña minus El Niño MEM mean  $P - E$  pattern for the two centuries and the difference. The difference is only colored where significant at the 95% significance level using a two-sided t-test. The models show for both centuries the expected pattern with drying across the equatorial Pacific Ocean (but extending too far west compared to observations, e.g. Seager et al. (2005)) with increased  $P - E$  in the Pacific Intertropical Convergence Zone (ITCZ) and South Pacific Convergence Zone (SPCZ), over the maritime continent and eastern Indian Ocean and over the tropical Atlantic Ocean and tropical South America. There is also increased  $P - E$  over the Indian subcontinent and southern Asia as observed.

The change from the 20<sup>th</sup> to the 21<sup>st</sup> Century is an intensification of the ENSO-driven  $P - E$  anomaly over the tropical Pacific, the eastern equatorial Indian Ocean, in the SPCZ and over the northern equatorial Atlantic Ocean. On the other hand the change represents a weakening of  $P - E$  variability (change of opposite sign to the 20<sup>th</sup> Century pattern) over the southern equatorial Atlantic Ocean, on the northern flanks of the Pacific ITCZ region and over the western equatorial Indian Ocean. Because of the much smaller subtropical and extratropical  $P - E$  anomalies compared to their tropical counterparts, and because of the importance of the variability over land, the 20<sup>th</sup> Century  $P - E$  variability and 21<sup>st</sup> minus 20<sup>th</sup> Century changes are shown for Africa and Asia in Figure 4 and for North and South America in Figure 5. The changes over Africa do not represent either a systematic weakening or strengthening but are quite spatially variable. An interesting feature is the development of a coherent ENSO-driven  $P - E$  anomaly over the Sahel in the 21<sup>st</sup> Century that did not exist in the prior century in the models (though it does in observations (Giannini et al. 2003)). In East Africa the dry-wet north south dipole extending from Somalia to Mozambique intensifies significantly. Over central and northern India, Bangladesh and southeast Asia the ENSO-driven  $P - E$  anomaly intensifies to a statistically significant amount in the 21<sup>st</sup> Century.

Over North America (Figure 5) the ENSO-driven  $P - E$  anomaly strengthens in southern

281 Mexico, weakens from central Mexico to the southern U.S. and in the Pacific Northwest but  
282 strengthens in northern California and northeast North America. Although not clear in the  
283 figure, there is a modest northward extension of the region with negative  $P - E$  during La  
284 Niña events. Very little of these changes over North America achieve even modest levels  
285 of statistical significance and it is not clear that the models can reliably project changes at  
286 these spatial scales. For South America ENSO-driven  $P - E$  variability weakens in northeast  
287 Brazil and strengthens in southeast South America between  $20^\circ$  and  $30^\circ S$ , both differences  
288 being statistically significant at the 95% level.

289 *a. Contribution of dynamic and thermodynamic mechanisms to changes in interannual*  
290 *ENSO-driven  $P - E$  variability*

291 In many parts of the world modeled  $P - E$  variability intensifies as might be expected  
292 due to rising specific humidity but this is not a universal result with some areas of strong  
293 teleconnections to ENSO (e.g. southern North America and northeast Brazil) showing a  
294 weakening of interannual  $P - E$  variability. Next we examine the mechanisms responsible  
295 for the modeled ENSO-driven  $P - E$  variability and its change between the two centuries.  
296 Figure 6 shows the contribution of the mean circulation dynamics,  $\delta MCD$  term for the  
297 20<sup>th</sup> and 21<sup>st</sup> Centuries and the difference. This is the term that gives rise to ENSO-driven  
298  $P - E$  anomalies as a consequence of changes in atmospheric circulation working on the  
299 climatological humidity. Comparing to Figure 3 it is clear that the  $MCD$  term has the same  
300 global spatial pattern and amplitude as the  $P - E$  variability itself, for both centuries. That  
301 is, ENSO-driven  $P - E$  variability is to first order a consequence of circulation, not humidity,  
302 variability (Seager and Naik 2011), and this remains the case under climate change. In most  
303 areas the 20<sup>th</sup> to 21<sup>st</sup> Century change in  $\delta MCD$  amplifies the 20<sup>th</sup> Century pattern with the  
304 exception of the western tropical Indian and equatorial Atlantic Oceans where it contributes  
305 a weakening.

306 Figure 7 show the contribution of the thermodynamic term,  $\delta TH$ , to the ENSO-driven  
307  $P - E$  variability. This term is several times smaller than the  $\delta MCD$  term in both centuries.  
308 In regions of mean low level divergence, such as over the equatorial Pacific cold tongue,

309 negative specific humidity anomalies during La Niña events, and positive anomalies during  
310 El Niño events, creates a tendency to positive  $P - E$  anomalies that weakly offset the  $\delta MCD$   
311 contribution. An opposite sign  $\delta TH$  contribution is over the western equatorial Pacific where  
312 the mean low level flow is convergent.

313 The change from the 20<sup>th</sup> to 21<sup>st</sup> Century of the  $\delta TH$  term is extremely small (Figure 7,  
314 bottom) (although it has the same sign as its 20<sup>th</sup> Century pattern as expected from rising  
315 humidity) and will be discussed no more. On the other hand the change in the pattern of  
316 ENSO-driven  $P - E$  variability is almost entirely accounted for by the change in the  $\delta MCD$   
317 contribution (Figure 6, bottom). That is, just as circulation variability creates the global  
318 pattern of  $P - E$  variability, so it is that changes in the circulation variability contribution  
319 cause the 20<sup>th</sup> to 21<sup>st</sup> Century change. Of course there will be a thermodynamic contribution  
320 to the change in  $\delta MCD$  as unchanged circulation anomalies become more effective in a  
321 moistening atmosphere. Hence we next break down  $\delta MCD$  into its two constituent parts as  
322 in Eqs. 14-16.

323 Figure 8 shows the change in the  $\delta MCD$  term and contributions to this from the change  
324 in specific humidity, working with the unchanged circulation variability, and the change in  
325 circulation variability, working with the unchanged specific humidity. Reassuringly so, the  
326 term that reflects the impact of rising specific humidity simply acts to amplify the  $\delta MCD$   
327 term and, hence, the  $P - E$  variability. However the term that reflects the change in ENSO-  
328 driven circulation variability is in many locations as large as, or larger than, the term with the  
329 mean humidity increase. For example this term creates the north-south dipole in the change  
330 in  $P - E$  variability over the tropical Atlantic and contributes significantly to the change in  
331  $P - E$  variability over the Indian Ocean. It also adds to the impact of rising humidity by  
332 increasing the strength of the negative  $\delta MCD$  term over the central equatorial Pacific Ocean  
333 and of the positive  $\delta MCD$  term over the maritime continent region. In the northern Pacific  
334 ITCZ region the change in the  $\delta MCD$  term is negative, which represents a weakening of  
335 the  $\delta MCD$  term, and this is caused by a weakening of the circulation anomaly. In contrast  
336 in the South Pacific Convergence Zone the change in the  $\delta MCD$  term is a strengthening of  
337 the contribution to positive  $P - E$  anomalies and this is caused by a strengthening of the  
338 circulation variability.

339 *b. Relationship of changes in the dynamic contribution to ENSO-driven interannual  $P - E$*   
340 *variability to changes in vertical velocity variability*

341 So far we have shown that ENSO-driven  $P - E$  variability is dominated by circulation  
342 variability working on the climatological specific humidity, that the 20<sup>th</sup> to 21<sup>st</sup> Century  
343 rise in humidity creates a tendency to more extreme  $P - E$  variability but that this can be  
344 interfered with by changes in the circulation variability itself. The importance of vertical  
345 motion in determining the horizontal moisture convergence and divergence anomalies that  
346 control  $P - E$  anomalies suggests that we may be able to better understand the changes  
347 in the dynamic contribution to  $P - E$  variability by examining vertical velocity variability.  
348 Figure 9 shows the MEM ENSO-driven variability of the vertical pressure velocity at 700mb  
349 for the 20<sup>th</sup> and 21<sup>st</sup> Centuries and the difference. The vertical pressure velocity has been  
350 multiplied by minus one so that positive is upward and so that the color scale matches that  
351 for  $P - E$  (green-wet-upward motion, brown-dry-downward motion). The difference is also  
352 plotted in contours on top of the 20<sup>th</sup> Century values in colors (bottom panel).

353 During model La Niñas, relative to El Niños, there is descending motion across the  
354 equatorial Pacific Ocean with ascending motion in the ITCZ region to the north and the  
355 SPCZ region to the southwest and also over the maritime continent-eastern Indian Ocean  
356 region. There is also widespread descent in the subtropics to mid-latitudes, including over  
357 southern North America. These model patterns are quite similar to observed patterns and  
358 are related to widespread subtropical to mid-latitude drought during La Niñas (Seager et al.  
359 2003, 2005; Seager 2007). The change in vertical velocity variability from the 20<sup>th</sup> to the 21<sup>st</sup>  
360 Century has some character of a reduction in amplitude, for example in the north Pacific  
361 ITCZ region and over the West Pacific warm pool and over the equatorial Atlantic Ocean.  
362 Elsewhere, increases in amplitude occur over the central equatorial Pacific Ocean (indicative  
363 of an eastward shift of ENSO-forced vertical velocity variability), over the Atlantic at about  
364 10°N and over the eastern equatorial Indian Ocean. There is also a notable weakening of  
365 the amplitude of vertical velocity variability over southern North America.

366 The spatial pattern of change in vertical velocity variability is very similar to that of the  
367 variable circulation contribution to the  $\delta MCD$  term (Figure 8, bottom) indicating that the

368 latter is closely controlled by the former. Given the strength of the contribution of change in  
369 circulation variability to the change in  $P - E$  variability, the pattern of the change in vertical  
370 velocity variability is also quite similar to the pattern of the change in the total  $\delta MCD$  term  
371 (Figure 6, bottom).

372 It has been well established that the mean tropical circulation weakens as a consequence of  
373 global warming (Vecchi and Soden 2007) which can be explained in terms of energy balance  
374 constraints when specific humidity rises at a faster rate than surface evaporation  
375 (Betts and Ridgway 1989; Betts 1990, 1998; Held and Soden 2006). It might be thought that  
376 these same constraints would cause ENSO-driven vertical motion anomalies to weaken. Since  
377 teleconnection patterns to higher latitudes are fundamentally driven by upper tropospheric  
378 divergent wind anomalies (Sardeshmukh and Hoskins 1988; Trenberth et al. 1998) this could  
379 then lead to weaker forced Rossby wave trains and associated circulation anomalies. This  
380 however does not appear to be generally the case. Circulation variability instead changes in  
381 a more complex manner probably related to changes in the location of ENSO SST anomalies,  
382 the basic state that impacts both the Rossby wave source and the flow through which Rossby  
383 waves propagate and the transient eddy-mean flow interaction that strongly controls the  
384 extratropical wave response to ENSO (Hoerling and Ting 1994; Seager et al. 2010b; Harnik  
385 et al. 2010).

## 386 5. Conclusions

387 We have investigated whether global warming leads to an increase in the amplitude of  
388 interannual  $P - E$  variability. This might be expected because of the increase in water  
389 vapor content of the atmosphere which has been shown previously to cause an increase in  
390 climatological precipitation extremes with wet areas getting wetter and dry areas getting  
391 drier, a phenomenon also known as 'rich get richer' (Held and Soden 2006; Chou et al. 2009;  
392 Seager et al. 2010c). This is examined using IPCC AR4/CMIP3 simulations of the 20<sup>th</sup>  
393 Century and projections of the 21<sup>st</sup> Century with the A1B emissions scenario, evaluating  
394 variability over each entire century. The results are as follows:

- 395 • As expected the amplitude of total interannual  $P - E$  variability increases almost

396 everywhere across the planet. The highest increases, of 40% or more, are over the  
397 equatorial Pacific and at high latitudes. Increases of around 10% are more common  
398 elsewhere. Over the eastern subtropical Pacific Ocean, over the subtropical Atlantic  
399 and over southwestern North America  $P - E$  variability actually weakens. This spatial  
400 pattern is somewhat akin to the pattern of climatological  $P - E$  change. It is also similar  
401 to that of the change in lower tropospheric moisture content but more accentuated.  
402 In regions where the  $P - E$  variance increases less than the mean specific humidity it  
403 can be explained because of a near global decrease in the amplitude of (annual and  
404 monthly mean) vertical velocity variability. Vertical velocity variance does increase  
405 over the equatorial Pacific and at polar latitudes, all regions of maximum increases in  
406  $P - E$  variance.

- 407 • In the tropical Pacific region ENSO-driven  $P - E$  variance also increases from the 20<sup>th</sup>  
408 to the 21<sup>st</sup> Century by as much as a quarter. Elsewhere changes in ENSO-driven vari-  
409 ance are more complex. In the Indian subcontinent, southeast Asia and Indonesia there  
410 is also an increase. Over eastern Africa the north-south dry-wet dipole with centers  
411 in Somalia-Ethiopia and Kenya-Mozambique strengthens. A stronger Sahel variability  
412 also develops. Over Central America ENSO-driven variance increases while over south-  
413 ern North America it decreases but not by a statistically significant amount. Northeast  
414 Brazil experiences a statistically significant weakening of ENSO-driven variance.
- 415 • ENSO-driven  $P - E$  variance is overwhelmingly dominated by circulation anomalies  
416 working with the climatological mean specific humidity. I.e. it is 'dynamics dominated'  
417 with anomalies in the mean flow being primarily responsible. As specific humidity rises  
418 in a warmer atmosphere it would be expected that this mean circulation contribution to  
419  $P - E$  anomalies would strengthen. This is indeed the case. However the contribution  
420 from the change in the ENSO-driven circulation anomalies is just as important. It is  
421 this term that allows ENSO-driven  $P - E$  variance to decrease in amplitude, such as  
422 over the equatorial Atlantic Ocean and northeast Brazil and southern North America.
- 423 • The change in the contribution of circulation variability to ENSO-driven  $P - E$  variabil-  
424 ity is closely matched by the change in ENSO-driven 700mb vertical velocity variability.

425 Over the equatorial Pacific Ocean there is an eastward shift of the longitude of max-  
426 imum vertical velocity variance. This, however, does not translate into an eastward  
427 shift of the longitude of maximum  $P - E$  variance because the influence of the specific  
428 humidity increase is centered west of the dateline. Over the tropical Atlantic Ocean  
429 La Niña events are associated with equatorially symmetric anomalous ascent. In the  
430 21<sup>st</sup> Century this ascent anomaly weakens south of the equator but strengthens north  
431 of the equator creating the dipole of change in ENSO-driven  $P - E$  anomaly.

432 To summarize, on the interannual timescale the widely held belief that hydroclimate  
433 variability intensifies as a result of global warming is confirmed to be true, according to  
434 the models participating in CMIP3 and assessed by IPCC AR4. Only in a few, mostly  
435 subtropical, areas of the globe does the interannual variability of  $P - E$  weaken. The  
436 change in  $P - E$  variability should be underway if the models are correct. Figure 10 shows  
437 time series of the spatial averages of total variance of  $P - E$  evaluated in 20 year running  
438 windows (with data detrended within the window) for south Asia ( $65^\circ - 110^\circ E, 0^\circ - 25^\circ N$ ),  
439 southwest North America ( $125^\circ - 95^\circ W, 25^\circ - 40^\circ N$ ), northeast Brazil ( $60^\circ - 35^\circ W, 20^\circ - 5^\circ S$ )  
440 and southeast South America ( $65^\circ - 35^\circ W, 40^\circ - 20^\circ S$ ), using land areas only. Increased  
441 variances for southern Asia and southeast South America in the early part of the current  
442 century are marked but the decreases in northeast Brazil and southwest North America  
443 are more modest. The dominant global mode of hydroclimate variability is ENSO which is  
444 also the only mode to possess proven predictability on the seasonal to interannual timescale.  
445 ENSO-driven  $P - E$  variability in the models does not increase uniformly, and in some places  
446 weakens, because of changes in the ENSO-driven circulation variability.

447 It is not understood why the total and ENSO-driven vertical velocity anomalies change  
448 in the way they do. However it is not fully understood why the observed or modeled 20<sup>th</sup>  
449 Century ENSO-driven vertical motion velocities have the spatial patterns and magnitudes  
450 that they do (see Seager et al. (2005)). Hence it seems premature to explain the 20<sup>th</sup> to 21<sup>st</sup>  
451 Century change in vertical velocity variability. More work is needed to better understand the  
452 coupling between dynamics and thermodynamics that determines circulation and precipita-  
453 tion variability and how this depends on the changing mean climate. Here we just note that  
454 in considering the primary potentially predictable component of  $P - E$  variability caution

455 is in order in anticipating how it will change. Since it is caused by circulation variability,  
456 changes in intra-tropical and tropical to extratropical teleconnections can cause altered lo-  
457 cations and amplitudes of ENSO-driven  $P - E$  anomalies. But it must be remembered that  
458 ENSO itself, and the regional details of ENSO-driven  $P - E$  anomalies, are not always well  
459 represented in the model simulations of the current climate and modeled changes in these in  
460 response to rising greenhouse gases contain uncertainty. However in some important places,  
461 such as most of southern Asia, the models do suggest that total hydroclimate variability, and  
462 its ENSO-driven component, strengthen from the 20<sup>th</sup> to the 21<sup>st</sup> Century. This is one of  
463 many regions of the world where natural variability of climate already wreaks havoc in terms  
464 of floods, droughts, crop failures, food shortages, and loss of human life. According to the  
465 model results presented here, quite apart from any change in mean climate, the variability  
466 of climate, no longer natural but a mixed hybrid of internal atmosphere-ocean variability  
467 and human-induced climate change, will only become more extreme amplifying stress on  
468 societies that are already hard pressed to cope with current day, more muted, variability.

469 *Acknowledgments.*

470 This work was supported by NOAA grants NA08OAR4320912 and NA10OAR4320137  
471 and NSF grant ATM-08-04107. LV was supported as a summer undergraduate intern at  
472 Lamont by NSF grant OCE-06-49024. The comments and advice of Lisa Goddard and  
473 Arthur Greene and the Global Decadal Hydroclimate (GloDecH) group at Lamont and  
474 Columbia were essential to the progress of this work.

## REFERENCES

- 477 Anyah, R. O., C. P. Weaver, G. Miguez-Macho, Y. Fan, and A. Robock, 2008: Incorporating  
478 water table dynamics in climate modeling: 3. Simulated groundwater influence on coupled  
479 land-atmosphere variability. *J. Geophys. Res.*, **113**, doi:10.1029/2007JD009087.
- 480 Betts, A. K., 1990: Greenhouse warming and the tropical water vapor budget. *Bull. Amer.*  
481 *Meteor. Soc.*, **71**, 1464–1465.
- 482 Betts, A. K., 1998: Climate-convection feedbacks: Some further issues. *Climatic Change*,  
483 **39**, 35–38.
- 484 Betts, A. K. and W. Ridgway, 1989: Climatic equilibrium of the atmospheric convective  
485 boundary layer over a tropical ocean. *J. Atmos. Sci.*, **46**, 2621–2641.
- 486 Cattiaux, J., R. Vautard, C. Cassou, P. Yiou, V. Masson-Delmonte, and F. Codron, 2010:  
487 Winter 2010 in Europe: A cold event in a warming climate. *Geophys. Res. Lett.*, **37**,  
488 doi:10.1029/2010GL044613.
- 489 Chou, C., J. D. Neelin, C. Chen, and J. Tu, 2009: Evaluating the 'rich-get-richer' mechanism  
490 in tropical precipitation change under global warming. *J. Climate*, **22**, 1982–2005.
- 491 Dole, R., et al., 2011: Was there a basis for anticipating the 2010 Russian heat wave?  
492 *Geophys. Res. Lett.*, **38**, doi:10.1029/2010GL046582.
- 493 Giannini, A., R. Saravanan, and P. Chang, 2003: Oceanic forcing of Sahel rainfall on inter-  
494 annual to interdecadal timescales. *Science*, **302**, 1027–1030.
- 495 Groisman, P. Y., R. W. Knight, D. R. Easterling, T. R. Karl, G. C. Hegerl, and V. N.  
496 Razuvaev, 2005: Trends in intense precipitation in the climate record. *J. Climate*, **18**,  
497 1326–1350.

498 Harnik, N., R. Seager, N. Naik, M. Cane, and M. Ting, 2010: The role of linear wave  
499 refraction in the transient eddy-mean flow response to tropical Pacific SST anomalies.  
500 *Quart. J. Roy. Meteor. Soc.*, 2132-2146.

501 Held, I. M. and B. J. Soden, 2006: Robust responses of the hydrological cycle to global  
502 warming. *J. Climate*, **19**, 5686–5699.

503 Hoerling, M. P. and M. Ting, 1994: Organization of extratropical transients during El Niño.  
504 *J. Climate*, **7**, 745–766.

505 Huang, H., R. Seager, and Y. Kushnir, 2005: The 1976/77 transition in precipitation over  
506 the Americas and the influence of tropical SST. *Clim. Dyn.*, **24**, 721–740.

507 Intergovernmental Panel on Climate Change, 2007: *Climate Change: The IPCC Scientific*  
508 *Assessment*. Cambridge University Press, Cambridge, England, 365 pp.

509 Koster, R. et al., 2004: Regions of strong coupling between soil moisture and precipitation.  
510 *Science*, **305**, 1138–1140.

511 Lo, M. and J. S. Famiglietti, 2011: Precipitation response to land subsurface hy-  
512 drologic processes in atmospheric general circulation models. *J. Geophys. Res.*, **116**,  
513 doi:10.1029/2010JD015134.

514 Meehl, G., C. Covey, T. Delworth, M. Latif, B. McAvaney, J. F. B. Mitchell, R. J. Stouffer,  
515 and K. E. Taylor, 2007: The WCRP CMIP3 multimodel dataset: A new era in climate  
516 change research. *Bull. Amer. Meteor. Soc.*, **88**, 1383–1394.

517 Neelin, J. D., M. Munnich, H. Su, J. E. Meyerson, and C. E. Holloway, 2006: Tropical drying  
518 trends in global warming models and observations. *Proc. Nat. Acad. Sci.*, **103**, 6110–6115.

519 O’Gorman, P. and T. Schneider, 2009: The physical basis for increases in precipitation  
520 extremes in simulations of 21st-century climate change. *Proc. Nat. Acad. Sci.*, **106**, 14773–  
521 14777.

522 Pall, P., T. Aino, D. A. Stone, P. A. Stott, T. Nozawa, A. G. J. Hilberts, D. Lohmann, and  
523 M. R. Allen, 2011: Anthropogenic greenhouse gas contribution to flood risk in England  
524 and Wales in autumn 2000. *Nature*, **470**, 382–386.

525 Sarachik, E. S., 2011: The tools needed to provide information for adaptation to future cli-  
526 mate conditions. *Proceedings of the 2nd International Conference: Climate, Sustainability*  
527 *and Development in Semi-Arid Regions, August 16 - 20, 2010, Fortaleza - Ceara, Brazil*,  
528 in press.

529 Sardeshmukh, P. D. and B. J. Hoskins, 1988: The generation of global rotational flow by  
530 steady idealized tropical divergence. *J. Atmos. Sci.*, **45**, 1228–1251.

531 Seager, R., 2007: The turn-of-the-century North American drought: dynamics, global con-  
532 text and prior analogues. *J. Climate*, **20**, 5527–5552.

533 Seager, R., N. Harnik, Y. Kushnir, W. Robinson, and J. Miller, 2003: Mechanisms of hemi-  
534 spherically symmetric climate variability. *J. Climate*, **16**, 2960–2978.

535 Seager, R., N. Harnik, W. A. Robinson, Y. Kushnir, M. Ting, H. P. Huang, and J. Velez,  
536 2005: Mechanisms of ENSO-forcing of hemispherically symmetric precipitation variability.  
537 *Quart. J. Roy. Meteor. Soc.*, **131**, 1501–1527.

538 Seager, R., Y. Kushnir, M. Ting, N. Naik, and J. Nakamura, 2010a: Northern hemisphere  
539 winter snow anomalies: ENSO, NAO and the winter of 2009/10. *Geophys. Res. Lett.*, **37**,  
540 doi:10.1029/2010GL043830.

541 Seager, R. and N. Naik, 2011: A mechanisms-based approach to detecting recent anthro-  
542 pogenic hydroclimate change. *J. Climate*, in press.

543 Seager, R., N. Naik, M. A. Cane, N. Harnik, M. Ting, and Y. Kushnir, 2010b: Adjustment  
544 of the atmospheric circulation to tropical Pacific SST anomalies: Variability of transient  
545 eddy propagation in the Pacific-North America sector. *Quart. J. Roy. Meteorol. Soc.*,  
546 **136**, 277–296.

- 547 Seager, R., N. Naik, and G. Vecchi, 2010c: Thermodynamic and dynamic mechanisms for  
548 large-scale changes in the hydrological cycle in response to global warming. *J. Climate*,  
549 **23**, 4651–4668.
- 550 Seager, R., et al., 2007: Model projections of an imminent transition to a more arid climate  
551 in southwestern North America. *Science*, **316**, 1181–1184.
- 552 Seneviratne, S. I., D. Luthi, M. Litschi, and C. Schar, 2006: Land-atmosphere coupling and  
553 climate change in Europe. *Nature*, **443**, 205–209.
- 554 Trenberth, K., G. W. Branstator, D. Karoly, A. Kumar, N. Lau, and C. Ropelewski, 1998:  
555 Progress during TOGA in understanding and modeling global teleconnections associated  
556 with tropical sea surface temperature. *J. Geophys. Res.*, **103**, 14 291–14 324.
- 557 Trenberth, K., A. Dai, E. M. Rasmussen, and D. B. Parsons, 2003: The changing character  
558 of precipitation. *Bull. Amer. Meteor. Soc.*, **84**, 1205–1217.
- 559 Vecchi, G. A. and B. J. Soden, 2007: Global warming and the weakening of the tropical  
560 circulation. *J. Climate*, **20**, 4316–4340.
- 561 Webster, P. J., V. E. Toma, and H.-M. Kim, 2011: Were the 2010 Pakistan floods predictable.  
562 *Geophys. Res. Lett.*, **38**, doi:10.1029/2010GL046 346.

563  
564

Table 1: Information on models considered for this study  
Included models

	Model name	Country	Atmospheric resolution	run number 20c3m/sresa1b
1	BCCR:BCM2	Norway	T63	run1/run1
2	CCCMA:CGCM3-1-T47	Canada	T47	run1/run1
3	CCCMA:CGCM3-1-T63	Canada	T63	run1/run1
4	CNRM:CM3	France	T63	run1/run1
5	CSIRO:MK3	Australia	T63	run1/run1
6	GFLD:CM2	United States	$2.5^\circ \times 2^\circ$	run1/run1
7	GFLD:CM2-1	United States	$2.5^\circ \times 2^\circ$	run1/run1
8	NASA:GISS-EH	United States	$5^\circ \times 4^\circ$	run1/run1
9	NASA:GISS-ER	United States	$5^\circ \times 4^\circ$ (B-grid)	run1/run2
10	LASG:FGOALS-G1-0	China	T42	run1/run2
11	INGV:ECHAM4	Italy	T106	run1/run1
12	INM:CM3	Russia	$5^\circ \times 4^\circ$	run1/run1
13	IPSL:CM4	France	$2.5^\circ \times 3.75^\circ$	run1/run1
14	NIES:MIROC3-2-medres	Japan	T42	run2/run1
15	NIES:MIROC3-2-hires	Japan	T106	run1/run1
16	MPIM-ECHAM5	Germany	T63	run1/run1
17	MRI:CGCM2-3-2	Japan	T42	run1/run1
18	NCAR:CCSM3	United States	T85	run1/run1
19	UKMO:HADGEM1	United Kingdom	$1.875^\circ \times 1.25^\circ$	run1/run1

565

Excluded Models

Model name	Country	problem with data
CSIRO:MK3	Australia	no $p_s$ for 21c
NASA:GISS-AOM	United States	natural variability in 21c is unrealistic
CONS:ECHO-G	Germany/Korea	no monthly $q, u, v$
NCAR:PCM1	United States	unrealistic ENSO variability in Indian Ocean
UKMO:HADCM3	United Kingdom	no $q$ for 21c

566

567



569 **List of Figures**

## Change in P-E variance using 19 AR4 models

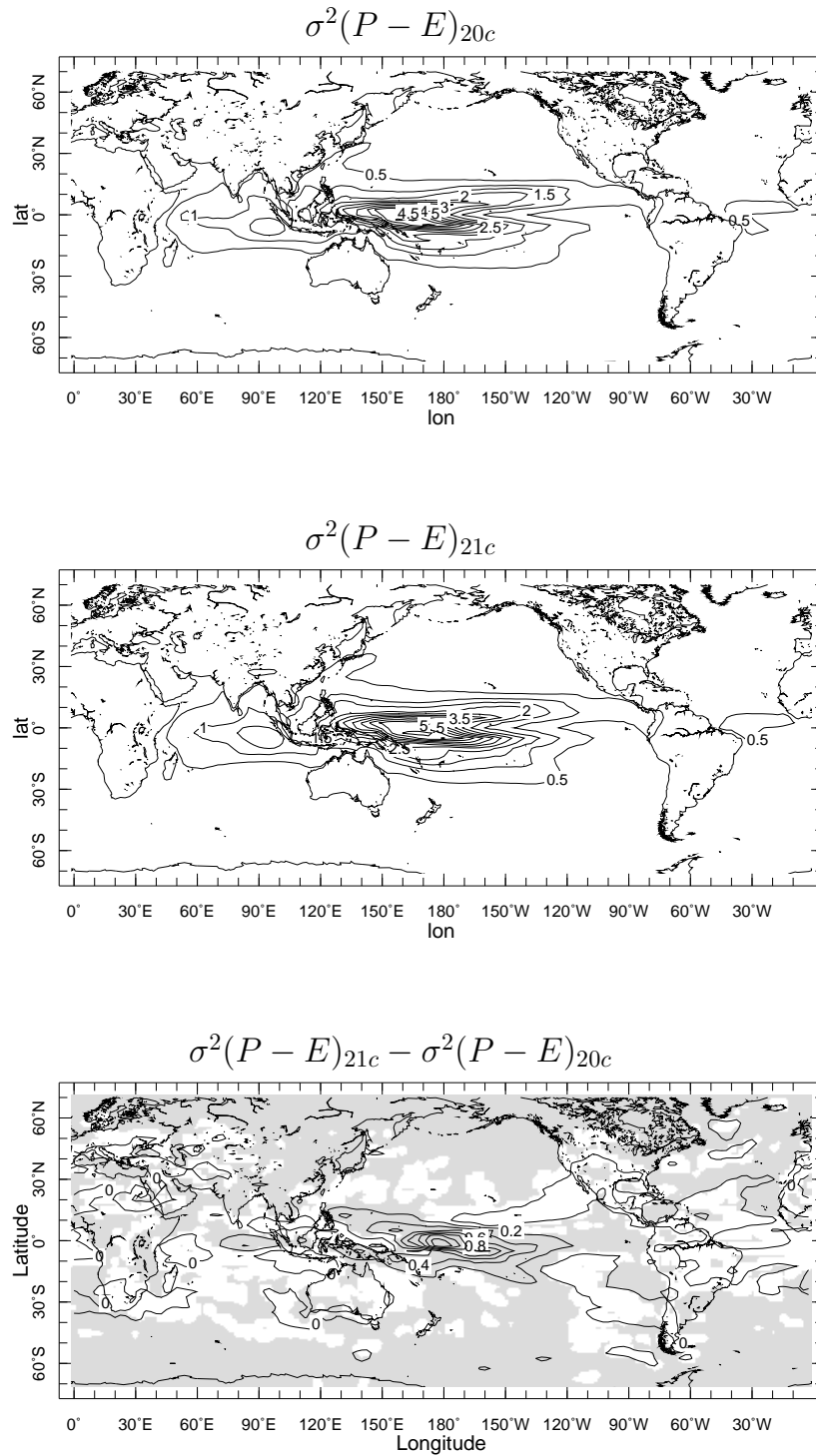
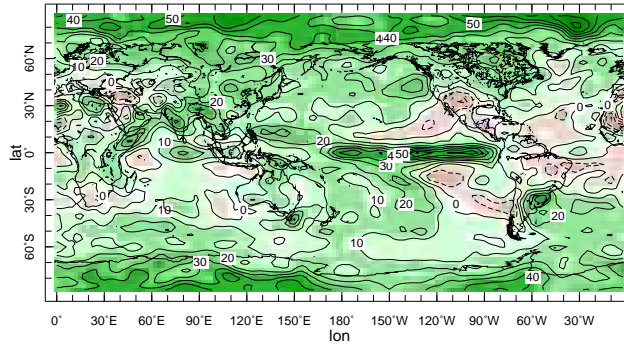
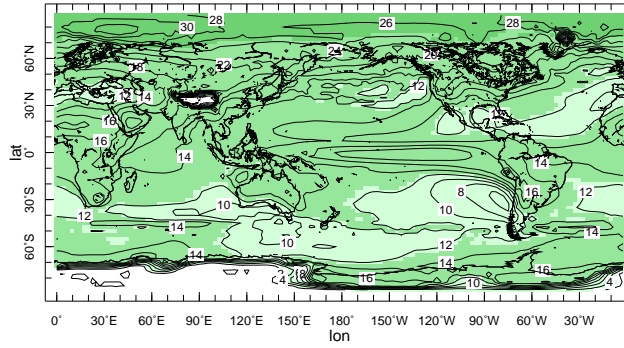


FIG. 1. The variance of annual mean  $P - E$  for the 20<sup>th</sup> Century (top), 21<sup>st</sup> Century (middle) and the difference (bottom) evaluated for each model and then averaged across the multi-model ensemble. Shading in the lower panel indicates significance at the 95% level. Units are mm/day squared.

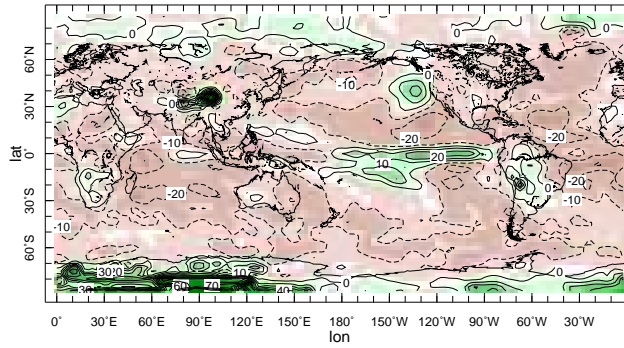
**% change in  $\sigma^2(P-E)$**



**% change in moisture, 1000mb to 700mb**



**% change in  $\sigma^2(\omega_{ANN})$**



**% change in monthly  $\sigma^2(\omega_{MON})$**

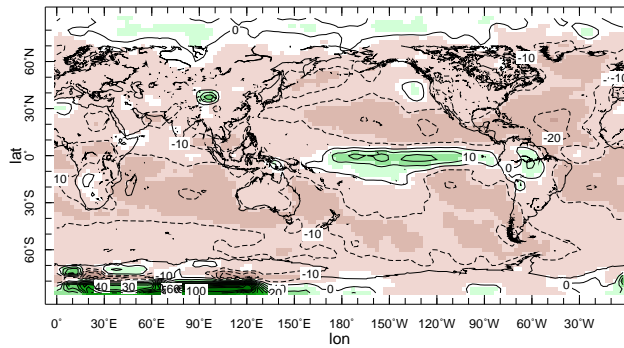
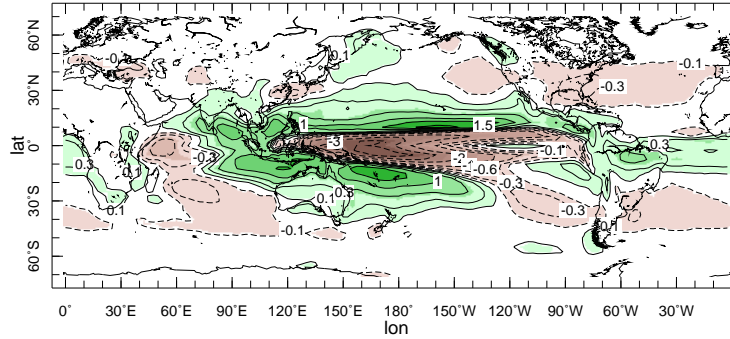


FIG. 2. The percent change in variance of the annual mean  $P-E$  field (top) and the percent change in the vertically integrated specific humidity (upper middle) with the percent changes in annual mean (lower middle) and monthly mean (bottom) vertical velocity variance for the multi-model ensemble.

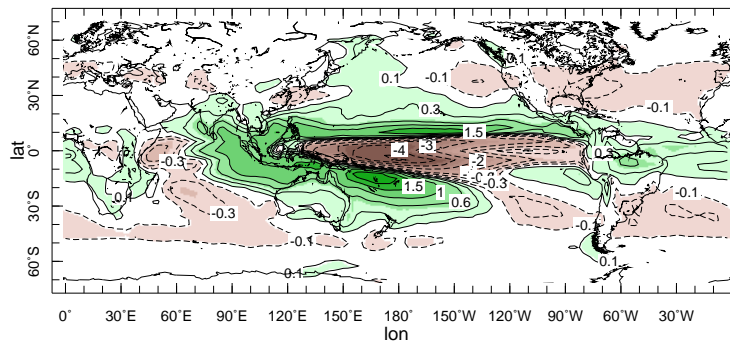
## Natural variability using 19 AR4 models

$$\delta(P - E)$$

20c: 1900 to 1999



21c: 2000 to 2099



21c-20c:

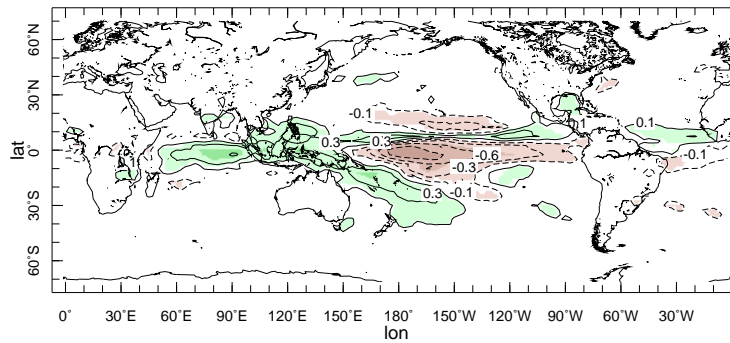
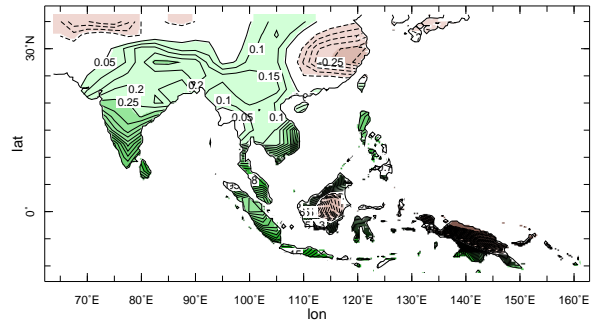
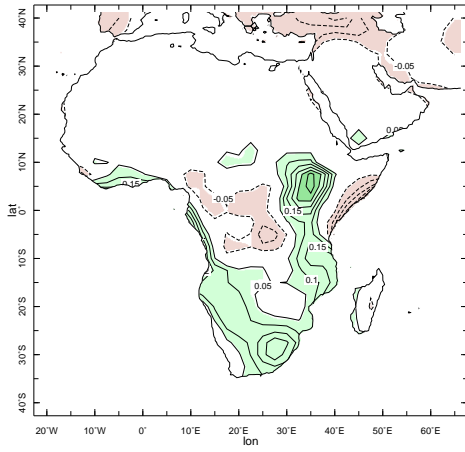


FIG. 3. The La Niña minus El Niño composite of  $P - E$  (mm/day) for the multi-model ensemble for the 20<sup>th</sup> Century (top), 21<sup>st</sup> Century (middle) and the difference (bottom). Colors are added where the difference is significant at the 95% level.

### 20<sup>th</sup>C ENSO-driven P-E variability



### 20<sup>th</sup>C to 21<sup>st</sup>C change

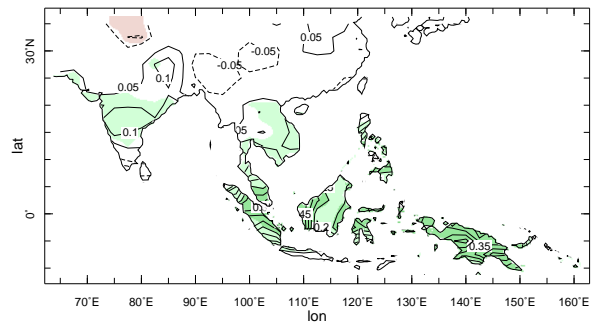
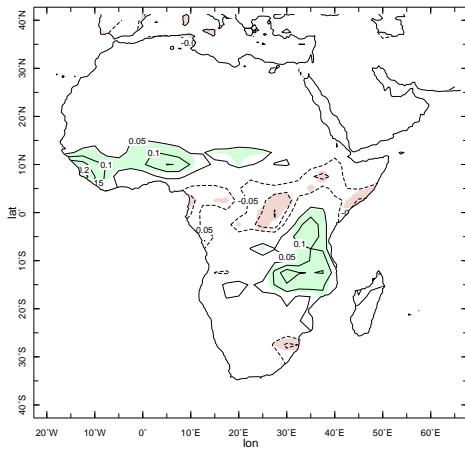
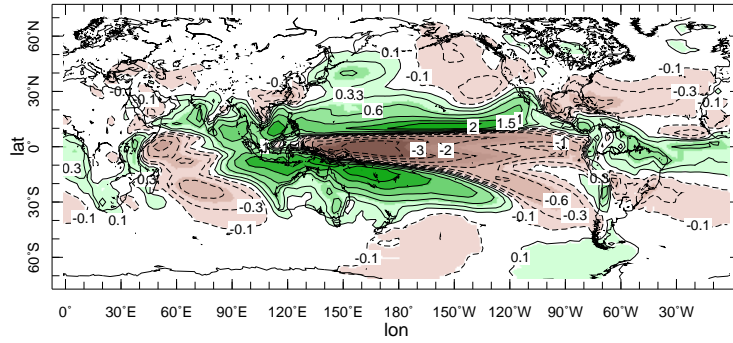


FIG. 4. As in Figure 3 but shown just for Africa and south Asia. Only regions where the difference is significant at the 95% level are colored.

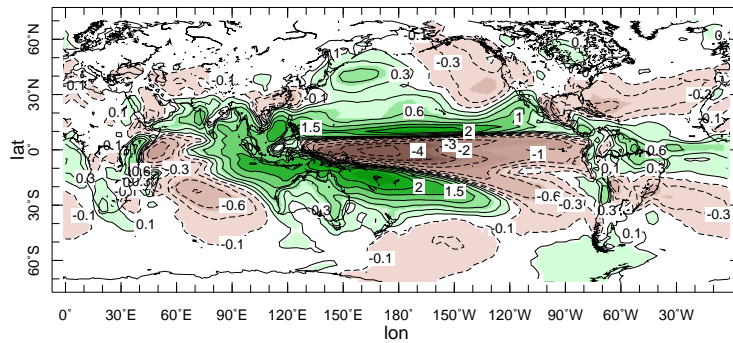


Natural variability using 19 AR4 models  
 $\delta MCD$

20c: 1900 to 1999



21c: 2000 to 2099



21c-20c(contours), 20c(colors)

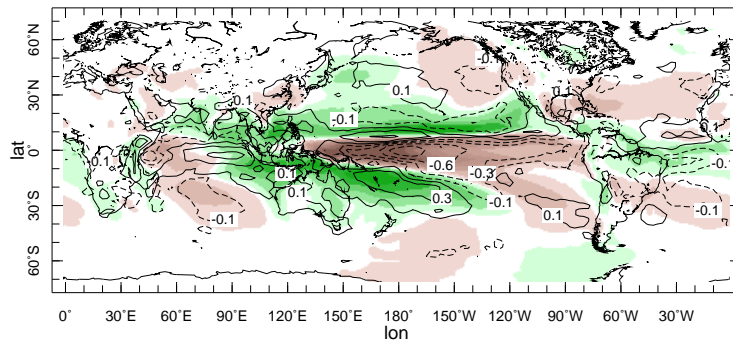
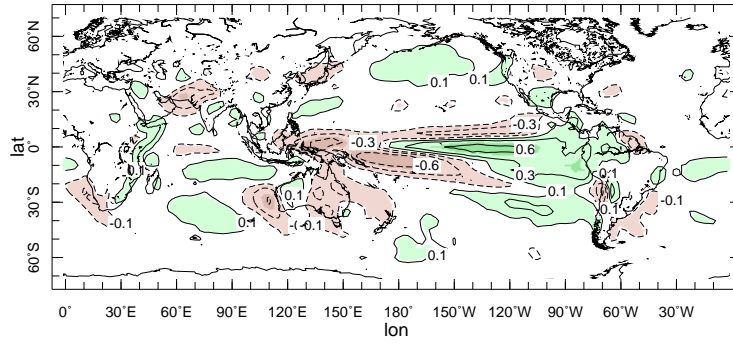


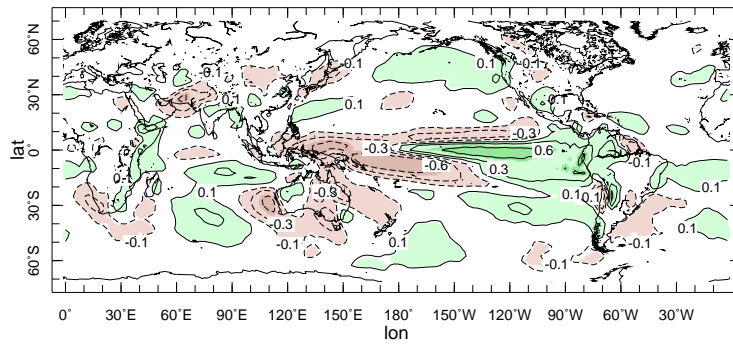
FIG. 6. The La Niña minus El Niño composite of the mean circulation dynamics ( $\delta MCD$ ) contribution to  $P - E$  variability for the multi-model ensemble for the 20<sup>th</sup> Century (top), 21<sup>st</sup> Century (middle) and the difference (bottom). Units are mm/day

Natural variability using 19 AR4 models  
 $\delta TH$

20c: 1900 to 1999



21c: 2000 to 2099



21c-20c(contours), 20c(colors)

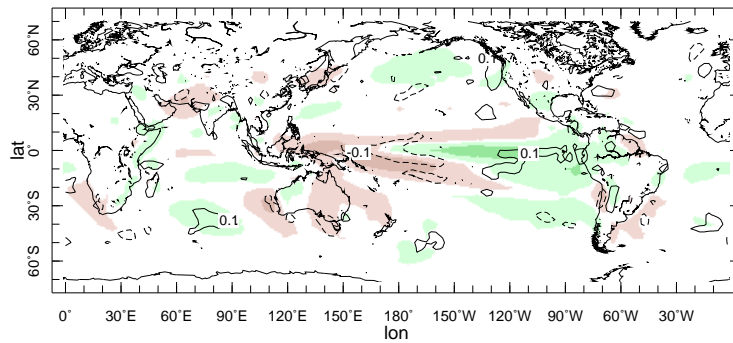


FIG. 7. Same as Figure 6 but for the thermodynamic ( $\delta TH$ ) contribution to the La Niña minus El Niño  $P - E$  composite. Units are mm/day

## Change in natural variability due to mean circulation dynamics

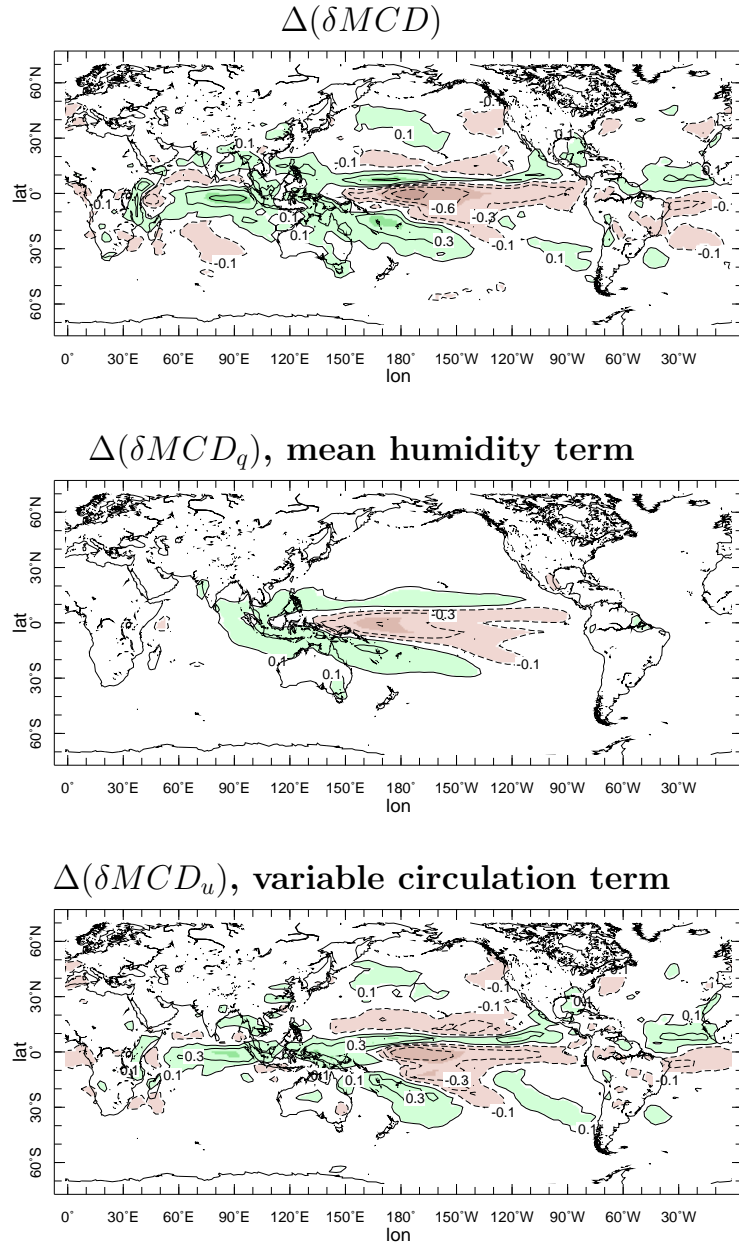


FIG. 8. The 21<sup>st</sup> minus 20<sup>th</sup> Century change in the La Niña minus El Niño composite of the mean circulation dynamics ( $\delta MCD$ ) contribution to  $P - E$  variability for the multi-model ensemble and the contributions to it from the change in mean specific humidity (middle) and the change in circulation variability (bottom). Units are mm/day

## Change in ENSO variability of 700mb vertical velocity

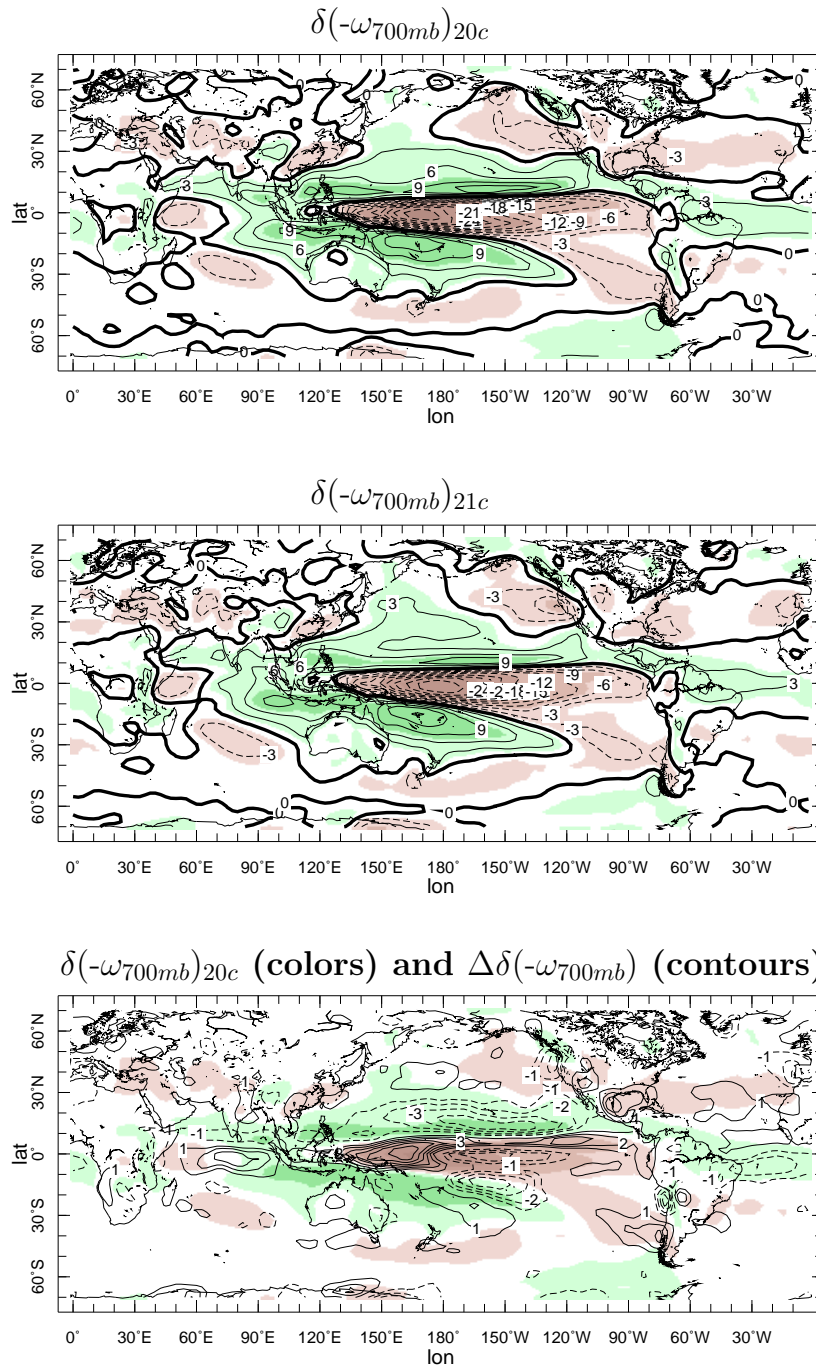


FIG. 9. The 20<sup>th</sup> (top) and 21<sup>st</sup> Century (middle) La Niña minus El Niño composite of the 700 mb vertical pressure velocity multiplied by minus one for the multi-model ensemble and the 21<sup>st</sup> minus 20<sup>th</sup> Century difference (contours) plotted on top of the 20<sup>th</sup> Century values (colors) (bottom). Units are mb/day

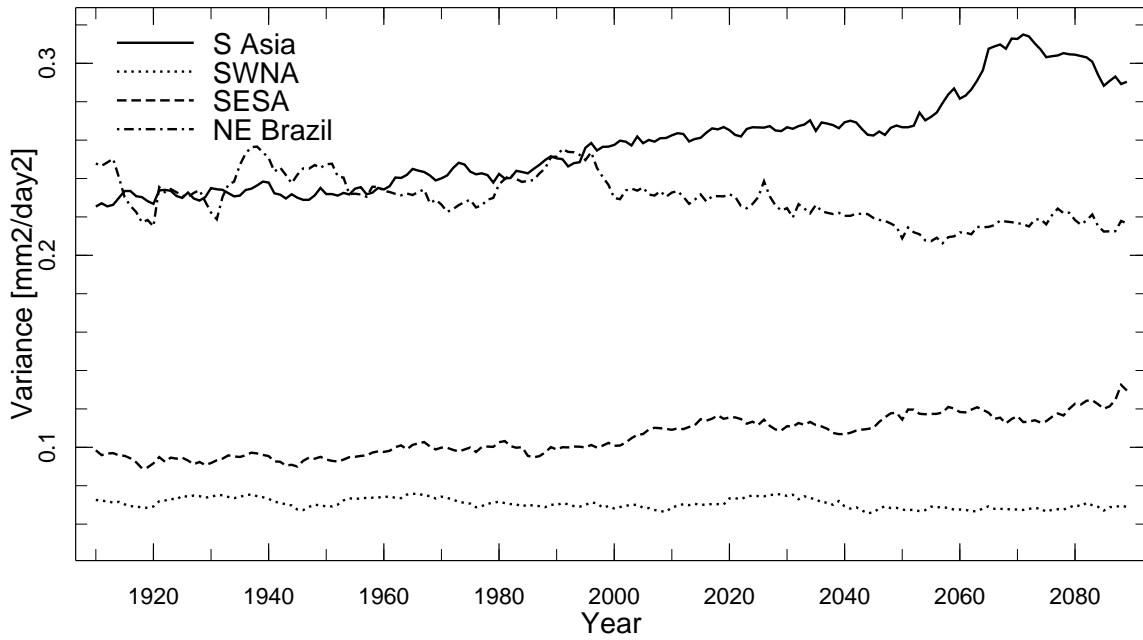


FIG. 10. The variance of  $P - E$  calculated in running 20 year windows for 1900 to 2100 with data detrended within the window for each grid point of each model and then averaged across models and across space for south Asia, southwest North America (SWNA), northeast Brazil and southeast South America (SESA). More details in text. Units are mm/day squared